Analysis of Resonance Between a VSC-HVDC Converter and the AC Grid

Changyue Zou, *Member, IEEE*, Hong Rao, *Senior Member, IEEE*, Shukai Xu, *Member, IEEE*, Yan Li, *Member, IEEE*, Weiwei Li, *Member, IEEE*, Jun Chen, *Member, IEEE*, Xiaobin Zhao, Yu Yang, and Bo Lei

***Abstract*—A 1270 Hz resonance occurred between ±350 kV/1000 MW Luxi back-to-back voltage source converter based high-voltage dc transmission (VSC-HVDC) converter and the 525 kV ac grid after disconnection of several ac transmission lines. To understand the resonance and find a solution, the impedance-based stability analysis model considering different equipment is first established. Then, the resonance is analyzed and repeated in the simulation based on the established model. The system stability can be judged by the ratio of grid impedance to the equivalent impedance of all parallel-connected equipment with the converter. To evaluate the occurrence and risk of resonance, the frequency range where the impedance has a negative-real-part has been searched and studied. In order to narrow the negative-real-part region to avoid potential resonance, solutions such as control strategy improvement and passive or active impedance adapter may be applicable and are discussed. For a complex system containing various equipment, the equipment can be divided into several subsectors to avoid modeling all possible combinations of equipment, which can be exhausting. And analysis has shown sufficient but not necessary condition to stabilize the system is to avoid the negative-real-part region in each sector.**

***Index Terms*—High-voltage dc transmission (HVDC) transmission, impedance, resonance, stability.**

I. Introduction

MODULAR multilevel converter (MMC) has been widely used in a high-voltage dc transmission (HVDC) system thanks to its modularity, strong expansibility, and low harmonic injection characteristics. The voltage source converter (VSC) based HVDC (VSC-HVDC) has recently attracted attention of researchers and been branded a highly available technology [1]–[5] in engineering field with numerous VSC-HVDC projects being planned or constructed worldwide. China has also experienced the growth in VSC-HVDC projects, including the ±30 kV/18 MW Nanhui project, the ±160 kV/200 MW Nan'ao multiterminal project, the ±200 kV/400 MW Zhoushan multiterminal project, the ±320 kV/1000 MW Xiamen project, and the ±350 kV/1000 MW Luxi back-to-back project. In addition, the ±500 kV/3000 MW Zhangbei dc-grid project and the ±800 kV/3000 MW/5000 MW Wudongde multiterminal LCC-VSC-UHVDC project have finished feasibility study and will soon head to the next phase.

With the dc voltage growing from 30 to 800 kV and capacity from 20 to 5000 MW, the VSC-HVDC has become a common part of the main grid, typically connecting the 525 kV ac grid through a transformer, thus facing much higher reliability requirement. Last year, a 1270 Hz resonance occurred between Luxi VSC-HVDC and the ac grid with the 1270 Hz phase-to-ground voltage reaching 68.9 kV. Although the power transmission and system stability were not interrupted, the resonance must be dealt with.

The system stability of a small-scale inverter has been widely studied. For inverters with an *LCL*-type filter, the oscillations effect of the *LCL* filter may lead to system instability. Generally, the system stability can be evaluated by the loop gain using Bode diagram or Nyquist stability criterion. To stabilize the system, passive damping [6]–[8] or active damping methods [9]–[12] are proposed to damp the inherent resonance. The main defects of passive damping methods, i.e., inserting a resistor in the filter, are the increment of loss and cost, which is unlikely to be applied in high-voltage large-capacity VSC-HVDC systems as a slight efficiency decrease will result in a considerable power loss. On the other hand, the active damping methods may fail or even deteriorate system stability after taking delay time into consideration, which has led to the proposal of active damping with reduced delay [13]. However, delay time of the VSC-HVDC system is much longer than that in small-scale converters, e.g., 400–600 μs, and is difficult to reduce, especially in existing systems. The influence of the grid impedance is ignored or modeled together with the grid-side inductance in the above-mentioned papers. But for VSC-HVDC connected to an HVAC system, it is hard to model them together as the grid impedance is usually quite complicated. Furthermore, the grid impedance can vary greatly along with a grid operation mode. Considering the changing nature of the grid operation mode, it is hardly applicable to consider all operation modes and repeat the stability analysis.

Another analytical procedure is to consider the inverter and the grid separately, e.g., the impedance-based stability criterion [14], [15]. Impedance-based stability criterion is established in [14]; conclusions show that the resonance between grid-connected inverters and the grid can be studied by applying the Nyquist stability criterion to the ratio of grid impedance

Manuscript received November 5, 2017; revised January 28, 2018; accepted February 12, 2018. Date of publication February 27, 2018; date of current version September 28, 2018. Recommended for publication by Associate Editor Xiongfei Wang. *(Corresponding author: Changyue Zou.)*

The authors are with the State Key Laboratory of HVDC, Electric Power Research Institute, China Southern Power Grid, Guangzhou 510080, China (e-mail: zoucy@csg.cn; raohong@csg.cn; xusk@csg.cn; liyan@csg.cn; liww@csg.cn; chenjun2@csg.cn; zhaoxb@csg.cn; yangyu@csg.cn; leibo@csg.cn).

Color versions of one or more of the figures in this paper are available online at http://ieeexplore.ieee.org.

Digital Object Identifier 10.1109/TPEL.2018.2809705

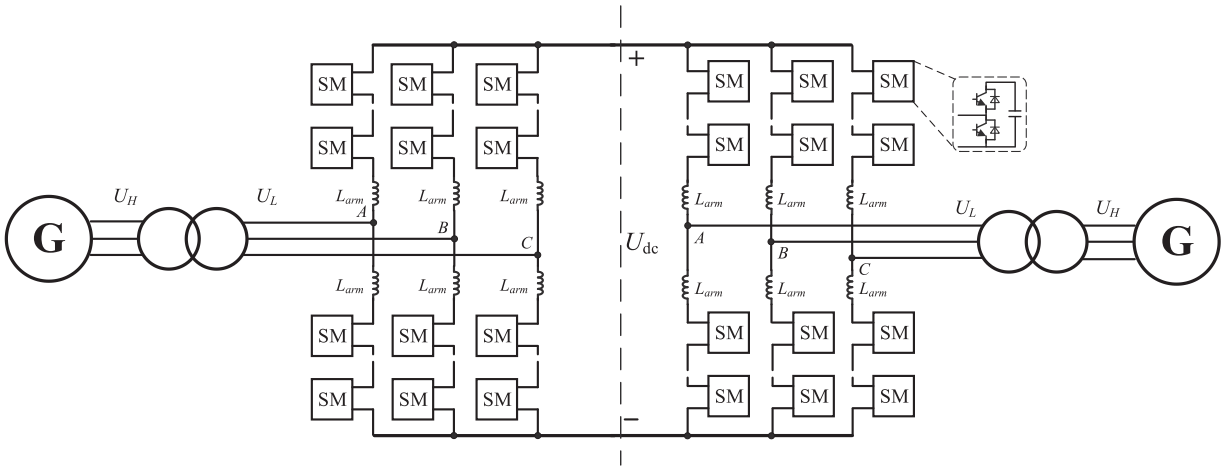

Fig. 1. Topology of the discussed VSC-HVDC.

and inverter impedance [16]. This method can be applied to analysis where the ac system is complicated and hard to model together with the inverter as well as dc-side stability analysis [2]. Concentrating on the ac impedance characteristic of the VSC, Prof. Lennart Harnefors has systematically studied the influence of the inner current controller and the outer loops controllers, e.g., phase-lock loop, direct-voltage controller, and alternating-voltage controller [17]–[21]. The system stability above the Nyquist frequency is furthered assessed in [22] by revisiting the modeling of a current control loop, especially the pulsewidth modulation and sampling process. Research results showed that the instability phenomena should not occur in frequencies where the ac impedance of the VSC has a positive-real-part [18]. Different methods of reshaping impedance to get a positive-real-part in the desired frequency regions by adjusting the controller parameters are provided in [17] and [20]. By reducing total delay time to 0.5*Ts*, a positive-real-part of the inner ac impedance is guaranteed [18] and the value considered in [19] and [20] is 1.5*Ts*. The delay time has a great influence on impedance characteristics [23] and longer delay time could deteriorate the system stability. This feature is more obvious in the VSC-HVDC case as the delay can be as long as 4 to 6*Ts*.

There are mainly two differences between VSC-HVDC and small-scale inverters: 1) The control delay is much longer, e.g., 400–600 μs, and damping strategies should be redesigned; and 2) The impedance of the high-voltage ac grid, e.g., 525 kV, may vary between capacitive and inductive when the operation mode changes. Such characteristics should be considered and evaluated in system stability analysis. The operation experience has shown that resonance can occur. The paper is organized as follows. The ac-side modeling of VSC-HVDC and impedance-based stability criterion considering multi-inverters and passive elements are established in Section II. The characteristic of grid impedance and VSC-HVDC impedance in the high-voltage application is introduced, and the mechanism of resonance is analyzed and discussed in Section III. The solutions are discussed in Section IV; particularly, the simplified method for stability analysis when lots of equipment are included is introduced. Finally, Section V draws a conclusion.

II. AC Impedance of VSC-HVDC and System Stability Criterion

A. AC-Side Modeling of VSC-HVDC

A half-bridge-based back-to-back VSC-HVDC topology is shown in Fig. 1. Thanks to the multilevel characteristics, no ac filter is necessary except for the arm inductor. Thus, the VSC-HVDC can be modeled as an inductor, which is equal to half of the arm inductor $L_{\rm arm}$ [24]. The ac impedance modeling of the VSC with *LCL* filters can be found in [23]. Recent research [25] showed that the dynamic behavior of submodules can affect the MMC model at low frequencies. The model in the high-frequency range is not as sensitive and is ignored as high-frequency resonance is analyzed in this paper. Generally, a transformer is necessary to match the ac and dc voltage and to satisfy the safety codes in an ultrahigh voltage system. Therefore, when modeling at the primary side, the VSC-HVDC is equivalent to an inductor, and its value is

$$L_{\rm VSC} = \frac{L_{\rm arm}}{2} \times \frac{U_H^2}{U_L^2} + L_{\rm leakage} \tag{1}$$

where $L_{\rm arm}$ is the arm inductance, $L_{\rm leakage}$ is the leakage inductance of the transformer at the primary voltage side, and U_H and U_L are the primary and secondary voltage of the transformer, respectively. The ac-side modeling of MMC VSC-HVDC is similar to that of a 2-level inverter with an *L*-type filter.

In VSC-HVDC, the direct current control is widely used; the VSC-HVDC projects with indirect current control are not discussed in this paper. The active and reactive current reference generally comes from outer loop control. Different outer loop control configurations are possible, for example, the dc voltage control for I_d and the reactive power control for I_q deployed in the sending terminal, and the active power control for I_d and reactive power control for I_q applied in the receiving terminal. The bandwidth of outer loop and phase-lock loop is quite low and the influence is ignored to concentrate on the main influencing factor. The ac impedance modeling considering outer loop and phase-lock loop can be found in [15], [17], [26], and [27].

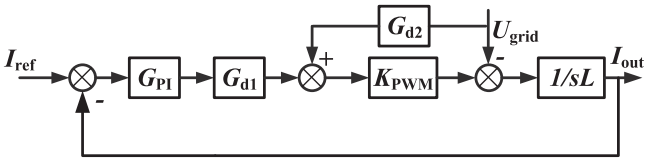

Fig. 2. Simplified control strategy applied in Luxi back-to-back VSC-HVDC.

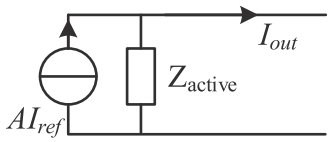

Fig. 3. AC-side equivalent model of VSC-HVDC.

Considering only the feedforward control and current inner loop control, the simplified control strategy is shown in Fig. 2.

The output current is given by

$$\begin{aligned} I_{\text{out}} &= AI_{\text{ref}} - U_{\text{grid}}/Z_{\text{active}} \\ &= \frac{G_{\text{PI}}G_{d1}}{sL + G_{\text{PI}}G_{d1}} I_{\text{ref}} - \frac{U_{\text{grid}}}{\frac{sL + G_{\text{PI}}G_{d1}}{1 - G_{d2}}} \end{aligned} \tag{2}$$

where A is the closed loop transfer function, and Z_{active} is the ac impedance of the VSC, also known as input impedance for the sending terminal or output impedance for the receiving terminal. G_{PI} is the PI controller of the current control loop, and K_{PWM} is the modulation factor, which is 1 here. G_{d1} and G_{d2} are the delay in forward and feedforward path, respectively. And

$$\begin{cases} G_{d1} = e^{-sT_{d1}} \\ G_{d2} = e^{-sT_{d2}} \end{cases} \tag{3}$$

where T_{d1} and T_{d2} are the time delay in forward and feedforward path, respectively. Generally, $T_{d1} = T_{d2}$, but they can be designed to be different [28]

$$G_{\text{open}} = \frac{G_{\text{PI}}G_{d1}}{sL}. \tag{4}$$

In order to keep the VSC-HVDC stable when connected to an ideal voltage source, the phase margin should be greater than zero. The control bandwidth can be estimated as follows. The phase of sL is $\pi/2$, the phase of G_{PI} vary from $-\pi/2$ to 0. The phase of G_d is

$$\varphi_{Gd1} = -2\pi f T_{d1}. \tag{5}$$

To get a $\pi/4$ phase margin, the maximum crossing frequency is estimated without consideration of phase correction control:

$$\text{PM} = \pi + \varphi_{\text{GPI}} + \varphi_{\text{Gd1}} - \varphi_{sL} = \frac{\pi}{4} \Rightarrow f_c = \frac{\varphi_{G\text{PI}}}{2\pi T_{d1}} + \frac{1}{8T_{d1}} \tag{6}$$

where φ_{GPI}, φ_{Gd1}, and φ_{sL} are the phase of the PI controller, G_{d1}, and sL, respectively, and PM is the phase margin.

When $T_{d1} = 100\,\mu$s, $f_{c\max} = 1.25$ kHz. When $T_{d1} = 600\,\mu$s, $f_{c\max} = 208.3$ Hz. The maximum crossing frequency is estimated supposing φ_{GPI} is zero, i.e., the corner frequency of the PI controller is much smaller. In engineering applications, the crossing frequency can be even smaller to get a larger phase margin. The time delay in high-voltage converters is much longer than that of small-scale systems due to the complexity of controlling several thousand MMC modules and multilevel control structure. Typical time delay can include the following parts.

1) Sampling of high-voltage current and the transmitting the measuring data to pole control, 76 μs.
2) Transmitting the data inside the pole control, 20 μs.
3) Filtering and synchronization of the measuring data, 90 μs.
4) Fulfilling pole control, 100 μs.
5) Transmitting modulation wave from pole control to valve control, 64.8 μs.
6) Transmitting the data inside valve control, 10 μs.
7) Fulfilling the valve control, 100 μs.
8) Sorting algorithm doing by field-programmable gate array and send to the distributed board, 50 μs.
9) Distributing driving signals, 20 μs.

Part of the delay can be reduced or eliminated by using faster CPU, better communication technology, or improved sequential logic, but time delay in VSC-HVDC is much larger than that of small-scale converters. The long delay greatly limits the bandwidth of VSC-HVDC systems although the controlling and sampling frequency is high, 10 kHz, for example.

According to (2), the VSC-HVDC can be modeled as a Norton branch judging from the ac side, as shown Fig. 3, where A and Z_{active} are given by (7).

When ignoring the outer loop, I_{ref} includes only fundamental reference and is an open loop for harmonics. The ac impedance can vary if the outer loop is considered. The outer loop is ignored in this paper as the bandwidth of the outer loop is much lower and contributes a little to harmonics, especially high-frequency harmonics

$$\begin{cases} A = \frac{G_{\text{PI}}G_{d1}}{sL + G_{\text{PI}}G_{d1}} \\ Z_{\text{active}} = \frac{sL + G_{\text{PI}}G_{d1}}{1 - G_{d2}} \end{cases}. \tag{7}$$

B. Impedance-Based System Stability Analysis

The ac side of the converter, whether the sending or receiving terminal of VSC-HVDC, can be substituted by a Norton branch when the current inner loop is applied. By substituting the ac grid by a Thevenin branch, an impedance-based system stability analytical model is obtained, as shown in Fig. 4. To make the analytical model universal, more than one converter is considered. In Fig. 4, Z_g represents the grid impedance, and Z_{active_n} and I_{0_n} are the ac impedance and the equivalent current source of the nth converter, as shown in Fig. 3. As ac filters are connected to the 525 kV grid in *LCC*-HVDC stations and a high-voltage inductor is frequently used to adjust the reactive power when necessary, passive elements are also included in the model.

For an ac grid branch

$$I_{\text{PCC}} = \frac{V_{\text{PCC}} - V_{\text{grid}}}{Z_g}. \tag{8}$$

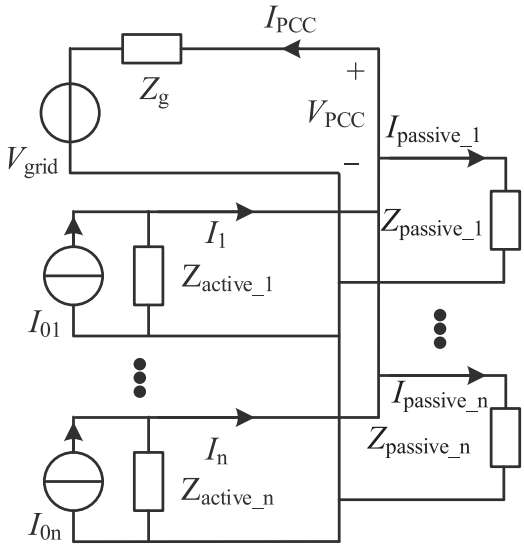

Fig. 4. Impedance-based system stability analytical model.

For a converter branch

$$I_n = I_{0\_n} - \frac{V_{\rm PCC}}{Z_{{\rm active}\_n}}. \tag{9}$$

The controlled current sources I_{0_n} and $Z_{{\rm active}\_n}$ are related to the control strategy of the converter. For a passive branch

$$I_{{\rm passive}\_n} = \frac{V_{\rm PCC}}{Z_{{\rm passive}\_n}}. \tag{10}$$

Applying the KCL theorem, we get

$$\sum I_n = I_{\rm PCC} + \sum I_{{\rm passive}\_n}. \tag{11}$$

Therefore, the PCC voltage is obtained

$$V_{\rm PCC} = \frac{V_{\rm grid} + Z_g \sum I_{0n}}{1 + \sum \frac{Z_g}{Z_{{\rm passive}\_n}} + \sum \frac{Z_g}{Z_{{\rm active}\_n}}}. \tag{12}$$

The system is stable provided that all the poles of (12) are in the left-half plane. I_{0_n} has no right-half plane pole, otherwise, the corresponding converter is unstable even when connecting to an ideal ac grid. Similarly, $V_{\rm grid}$ and Z_g have no right-half plane pole. Consequently, the system stability can be judged by applying Nyquist stability criterion to part of the denominator, i.e.,

$$G_{\rm stability} = \sum \frac{Z_g}{Z_{{\rm passive}\_n}} + \sum \frac{Z_g}{Z_{{\rm active}\_n}} = \frac{Z_g}{Z_{\rm eq}} \tag{13}$$

where $Z_{\rm eq}$ is the impedance of all the parallel-connected elements

$$Z_{\rm eq} = \frac{1}{\sum \frac{1}{Z_{{\rm passive}\_n}} + \sum \frac{1}{Z_{{\rm active}\_n}}}. \tag{14}$$

When more than one active or passive elements are connected at PCC in parallel, the system stability can be judged by the ratio of the grid impedance to the impedance of all the parallel-connected elements. When only one converter and no passive element are connected to the grid, the stability transfer function

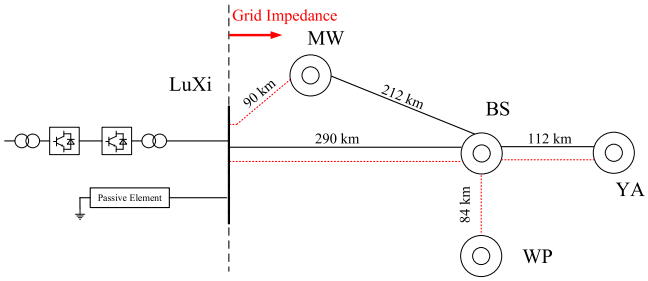

Fig. 5. AC network of the Guangxi-side of Luxi district.

is simplified as

$$G_{\rm stability} = \frac{Z_g}{Z_{\rm active}} = \frac{Z_g}{\frac{sL + G_{\rm PI} G_{d1}}{1 - G_{d2}}}. \tag{15}$$

According to the Nyquist stability criterion, there are two typical sufficient but not necessary conditions to keep the system stable.

The first one is the phase condition, i.e., the system is stable if the phase difference of Z_g and $Z_{\rm eq}$ is smaller than 180° for all frequencies. It means that the stability can be guaranteed if the real-part or imaginary-part of Z_g and $Z_{\rm eq}$ has the same polarity for all frequencies.

The second one is the magnitude condition, i.e., the system is stable if the magnitude of Z_g is smaller than that of $Z_{\rm eq}$ for all frequencies, which guaranteed the magnitude of $G_{\rm stability}$ is always smaller than 0 dB.

III. Resonance Between the VSC-HVDC and AC Grid

A. Characteristic of AC Impedance of a High-Voltage AC Grid

The structure of the 525 kV ac grid at the Guangxi-side, where the resonance discussed in this paper occurred, is shown in Fig. 5. The detailed modeling of the ac network is out of this paper's scope, as a result, the grid impedance is scanned and given here. The grid impedance scan method can be found in [29]. The scanned results illustrated below are used to show characteristics of the grid impedance vividly and are not used for further study. The grid impedance when all ac lines are in service and when the dashed red-lines are out of service are scanned and shown in Fig. 6.

According to the scanned grid impedance result, the magnitude of Z_g can be very large at resonance frequencies and resonance frequency can vary along with the operation mode. It is hard to keep the magnitude of $Z_{\rm active}$ larger than Z_g at all frequencies, especially when the short-circuit ratio is small. Therefore, the magnitude condition discussed in Section II-B is hardly applicable in large-scale VSC-HVDC projects.

As for the phase condition, the grid impedance can be inductive or capacitive, i.e., the imaginary part of Z_g can be positive or negative. It is impossible to ensure that the imaginary part of $Z_{\rm active}$ and that of Z_g have the same polarity as the polarity of Z_g changes frequently along with the operation mode. Fortunately, without considering VSC-HVDC and distributed power generation system, the real-part of Z_g is always positive. As a result,

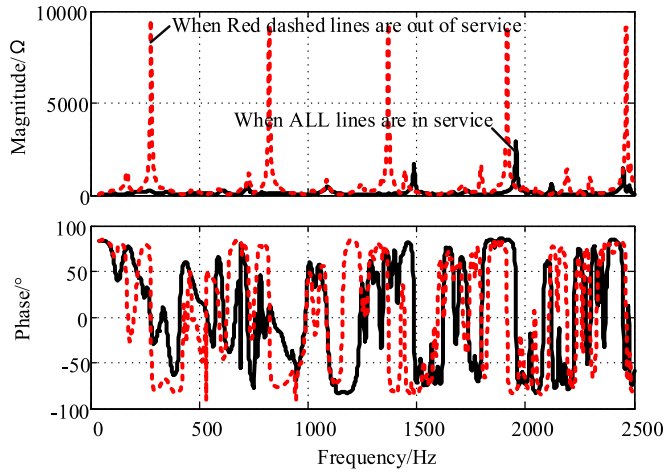

Fig. 6. Scanned ac grid impedance in two different operation modes.

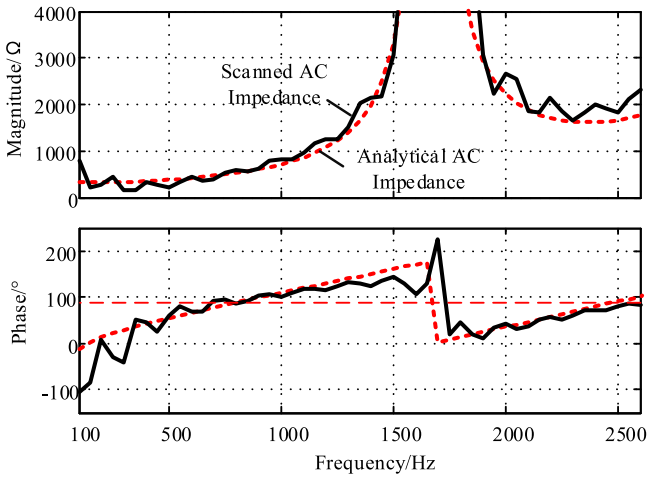

Fig. 7. Comparison of simulated and analytical ac impedance of VSC-HVDC.

TABLE I
PARAMETERS AND VALUES OF LUXI VSC-HVDC

Parameters		Value
Proportional gain of the current controller		50
Integral gain of the current controller		500
Arm inductor (L_{arm}/H)		0.14
Control delay in the forward path (T_{d1}/μs)		600
Control delay in the feedforward path (T_{d2}/μs)		600
DC voltage(U_{dc}/kV)		700
Transformer	Capacity (Per phase/MVA)	375
	Primary voltage (U_H/kV)	525
	Secondary voltage (U_L/kV)	375
	Leakage inductance (%)	14

the stability can be unconditionally guaranteed when Z_{active} has a positive-real-part for all frequencies.

B. VSC-HVDC AC Impedance Verification

To verify the ac impedance analytical results given by (7), the VSC-HVDC ac impedance is scanned in EMTDC/PSCAD. The control strategy, control parameters such as time delay, and transient processing logic are the same as those in the project. An ideal small harmonic voltage source is connected in series with a 525 kV/50 Hz ideal voltage source, and the simulation is repeated in a series of frequencies to get the scanned ac impedance curve. The key parameters and corresponding value of the VSC-HVDC project are listed in Table I. The scanned and analytical ac impedance are illustrated in Fig. 7.

The phase of VSC-HVDC ac impedance is above zero except for the frequencies lower than 200 Hz, i.e., the VSC-HVDC impedance shows inductive characteristic for mid- and high-frequencies. Therefore, no high-frequency resonance will occur if the grid remains inductive. Generally, the grid impedance is simplified as an inductor connected in series with a resistor during the design of control strategy and high-frequency resonance should not occur under such assumption. To analyze and detect the high-frequency resonance phenomena, the grid impedance should not be modeled as a resistor–inductor branch.

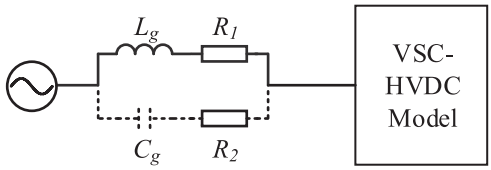

Fig. 8. Grid impedance structure.

TABLE II
PARAMETERS AND VALUES OF GRID IMPEDANCE IN SIMULATION

Parameters	Value
Inductance (L_g/mH)	169.3
Resistance of the inductor branch (R_1/Ω)	8.4
Capacitance (C_g/μF)	0.2
Resistance of the capacitor branch (R_2/Ω)	171.0

The system stability is guaranteed if the real-part of Z_{active} is positive for all frequencies. However, Z_{active} has a negative-real-part in quite a large range, which may cause instability while the phase difference between Z_g and Z_{active} is greater than 180°.

C. High-Frequency Resonance Simulation

To verify the high-frequency resonance analytical result, a simulation is conducted in EMTDC/PSCAD v4.6. The grid impedance is simulated by an inductive branch connected in parallel with a capacitive branch, as shown in Fig. 8. The parameters of Z_g are listed in Table II, where L and R_1 are the parameters of a weak ac grid when parasitic capacitance is ignored. The parameters of the VSC are listed in Table I.

The grid impedance and ac impedance of the VSC are illustrated in Fig. 9(a); there are two amplitude intersections at 276 and 1252 Hz. For the latter one, the phase difference of Z_g and Z_{active} is $-196°$. The ratio Z_g/Z_{active} crosses over $-180°$ from upper to lower when the magnitude is above zero, i.e., the system is unstable. The simulation result is shown in Fig. 10(a); the fast Fourier transform (FFT) analysis of phase B current is shown in Fig. 10(b); the 1250 Hz harmonic current gets larger gradually and finally trips the system. By reducing R_2, the

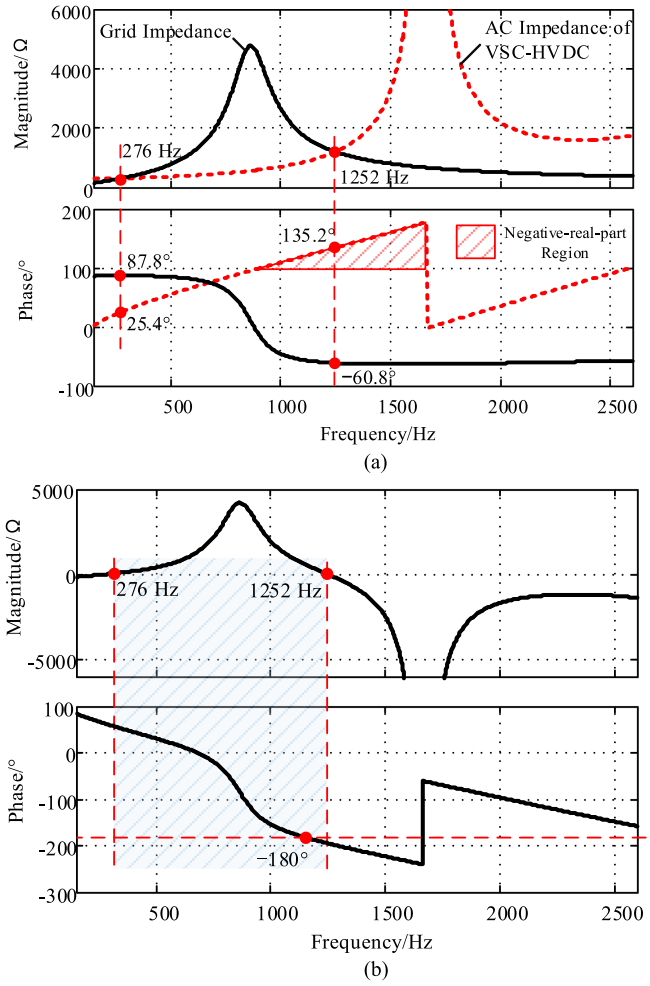

Fig. 9. Impedance analytical result. (a) Z_g and Z_{active}. (b) The ratio of Z_g and Z_{active}.

harmonic increasing rate gets larger. At 2.8 s, the capacitive branch is disconnected by a breaker, and the harmonic disappears immediately, as shown in Fig. 10(c). At 1250 Hz, the real-part of Z_{active} is negative, which is a necessary condition to destabilize the system. By adjusting parameters of L_g and C_g, the resonance frequency can be designed in the simulation. In industrial applications, the grid impedance changes along with the operation mode, but only limited cases are included in the analysis. However, by eliminating the negative-real-part region, an unconditional stability can be guaranteed.

D. Negative-Real-Part Region Analysis

Focusing on the negative-real-part region, parameters sensitivity of Z_{active} can be conducted. According to (7)

$$Z_{\text{active}}(\omega) = \frac{sL + G_{\text{PI}}G_{d1}}{1 - G_{d2}} = \frac{j\omega L + \left(K_p + \frac{K_i}{j\omega}\right)(\cos(\omega T_{d1}) - j\sin(\omega T_{d1}))}{1 - \cos(\omega T_{d2}) + j\sin(\omega T_{d2})}. \quad (16)$$

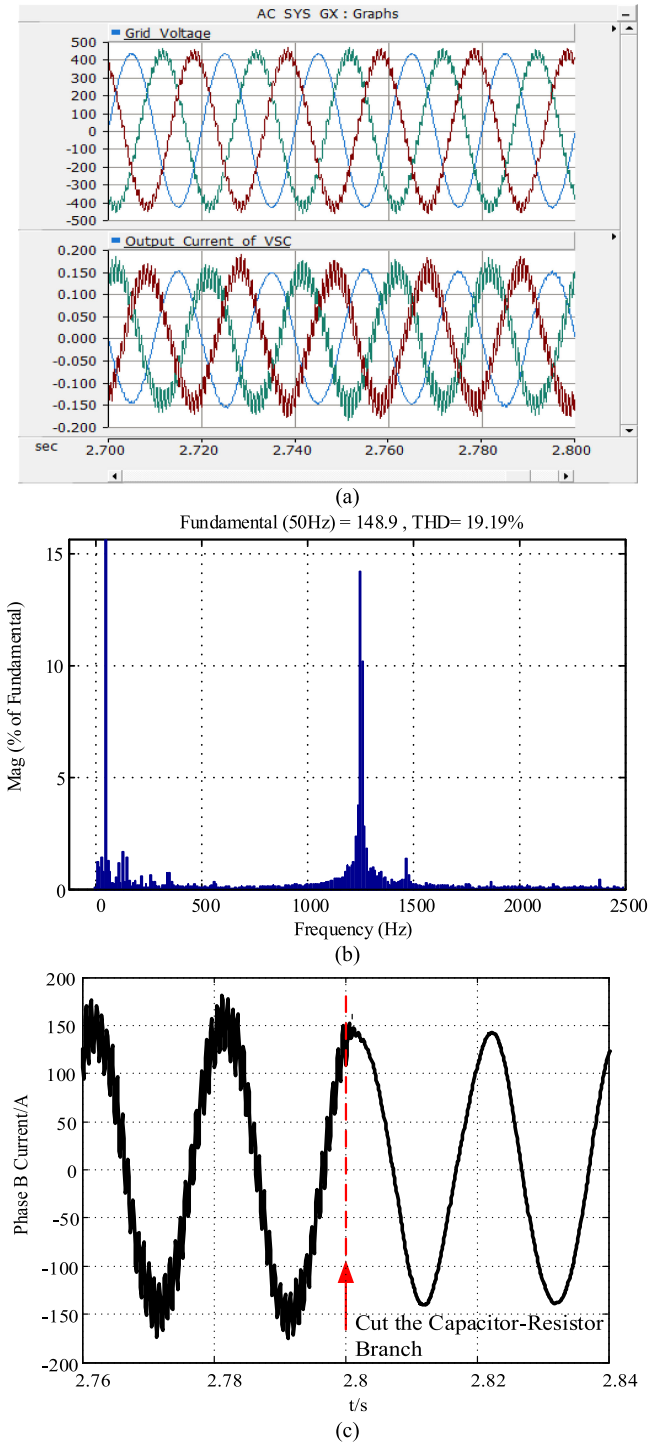

Fig. 10. Simulation result. (a) The grid voltage and the output current of the VSC. (b) The FFT analysis result of phase B current. (c) Cut the capacitor–resistor branch at 2.8 s.

The ac impedance of VSC-HVDC is affected by inductor L, PI controller parameters, and delay times T_{d1} and T_{d2}. The influence of G_{PI} is limited as controller parameters are limited by the phase margin requirement considering the long delay, as discussed in Section II-A, which makes the magnitude G_{PI} smaller than sL. The magnitude comparison of sL and $G_{\text{PI}}G_d$ is shown in Fig. 11. Consequently, the influence of T_{d1} is also limited.

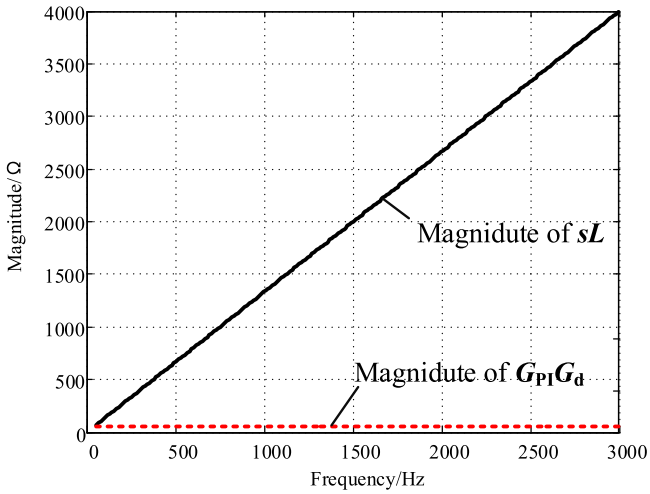

Fig. 11. Magnitude comparison of sL and $G_{\mathrm{PI}}G_d$.

The Bode diagram of Z_{active} considering different K_p and L is depicted in Fig. 12. The magnitude changes nearly proportional to L, but the negative-real-part region rarely changes when K_p or L changes. The similar analysis can be done to K_i and T_{d1} and similar conclusions are drawn. This is reasonable as control bandwidth is limited by the long delay, and the PI controller rarely responds to high-frequency signals; thus, Z_{active} has a low correlation with PI controller and T_{d1}.

Z_{active} when T_{d2} is 600 and 200 μs are calculated and depicted in Fig. 13(b). There are more than one resonance peaks in Z_{active} and the resonance frequencies f_r are n/T_{d2}, where n is integrals. The negative-real-part region changes completely when T_{d2} changes.

The variation of the denominator of Z_{active} is cycled with frequency $1/T_{d2}$, but the numerator gets larger along with frequency. The smaller the time delay T_{d2}, the higher the first resonance frequency $1/T_{d2}$, making magnitude of Z_{active} inside the first negative-real-part region larger. As a result, the resonance is less likely to occur because $|Z_g|/|Z_{\text{active}}|$ is more likely to be smaller than 0 dB. Although increasing L is also helpful, the increment of cost might not be appreciated.

The negative-real-part region of Z_{active} is highly related to delay in the feedforward path; the conclusion is correct when instantaneous feedforward control is applied as the feedforward control reacts to high-frequency signals. Consequently, one of the solutions is to add a low-pass filter in the feedforward path to narrow the negative-real-part region, this will be discussed in the following section.

By conducting negative-real-part region analysis, the major cause triggering the resonance could be found. Effective solutions could be found thereafter.

E. 1270 Hz *Resonance Occurred Between the ±350* kV/*1000* MW *VSC-HVDC and AC Grid*

The Luxi back-to-back station is located at the border intersection of Yunnan, Guangxi, and Guizhou province, and consists of 2 × ±160 kV/1000 MW *LCC* and 1 × ±350 kV/1000 MW VSC, as shown in Fig. 14. The topology and control strategy

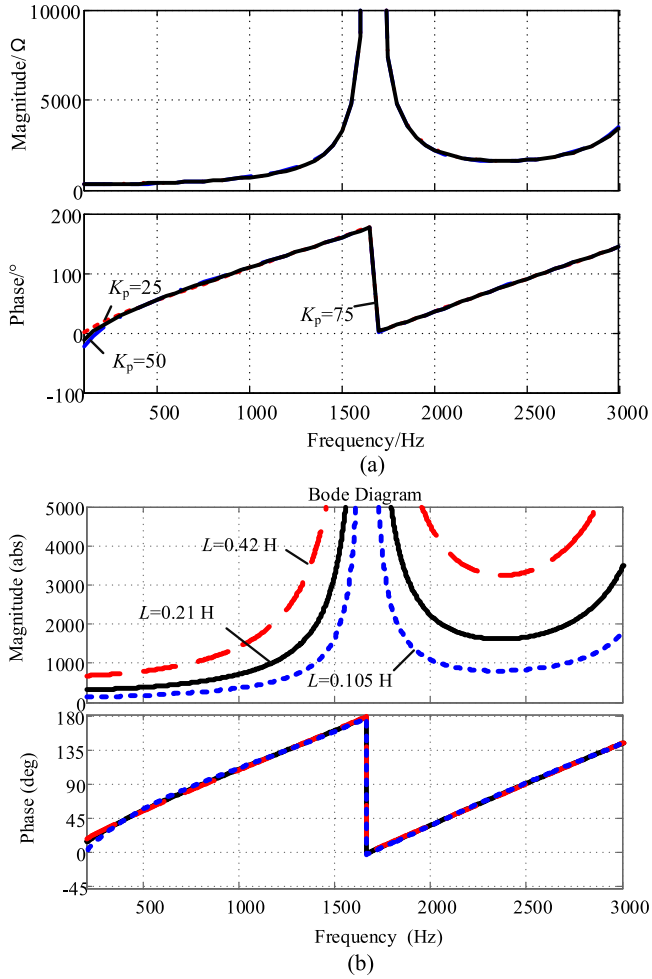

Fig. 12. AC impedance of VSC-HVDC considering different K_p and time delay T_{d2}. (a) Different K_p. (b) Different L.

are shown in Figs. 1 and 2. The project is built to separate the Yunnan grid to the rest of the CSG main grid in face of serious regional frequency imbalance. Although VSC-HVDC is capable of bidirectional power transmission, the main purpose of the project is transferring power from Yunnan-side to Guangxi-side.

During the operation of the project, a 1270 Hz resonance occurred at the Guangxi-side. In the LCC-HVDC, the related ac filters were not in service when the resonance occurred. The ac lines in the area were mostly out of service when the resonance occurred, as the red dashed lines shown in Fig. 5 and the short-circuit capacity is about 3.3 GVA. The harmonic keeps growing after the ac lines are cut off and then maintains at a certain level instead of making the system unstable directly. Some unknown nonlinear factor is thought to have stopped the harmonic from getting larger. The harmonic disappeared after the VSC-HVDC tripped. The grid voltage and the output current of the VSC when resonance maintained is shown in Fig. 15(a), and the FFT result of phase B current is depicted in Fig. 15(b). The 1270 Hz peak value of phase-ground voltage and phase current reached as high as 68.9 kV and 60.1 A. This is the first high-frequency resonance case observed in CSG. The high-frequency resonance is a threat to the system operation and should be dealt with.

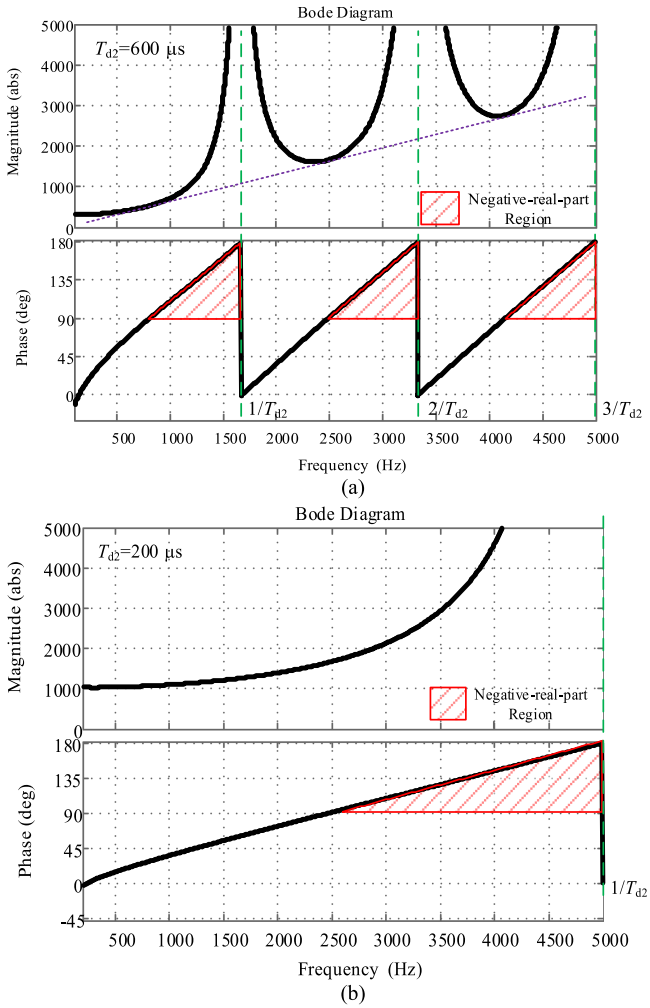

Fig. 13. AC impedance of VSC-HVDC when: (a) $T_{d2} = 600\,\mu$s and (b) $T_{d2} = 200\,\mu$s.

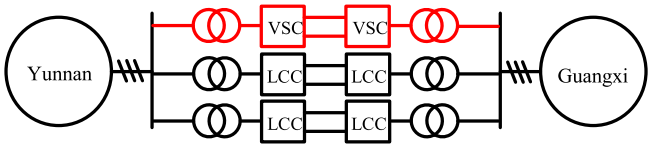

Fig. 14. Three back-to-back HVDC is built in parallel in the Luxi station.

According to the observed harmonic, the output impedance of VSC-HVDC at 1270 Hz is about 1145 Ω ∠ 133.9°, while the analytical impedance at 1270 Hz is 1281 Ω ∠ 137°. The analytical impedance is close to the observed value.

The Guangxi-side ac grid is modeled in PSCAD v4.6, and similar resonance can occur when the ac lines are cut off. The resonance frequency is about 1.1 kHz; several reasons may be responsible for the difference.

1) Only the 220 and 525 kV ac line are modeled.
2) The parameters of the ac transmission line may not be precise enough.
3) The ac loads model are ideal.

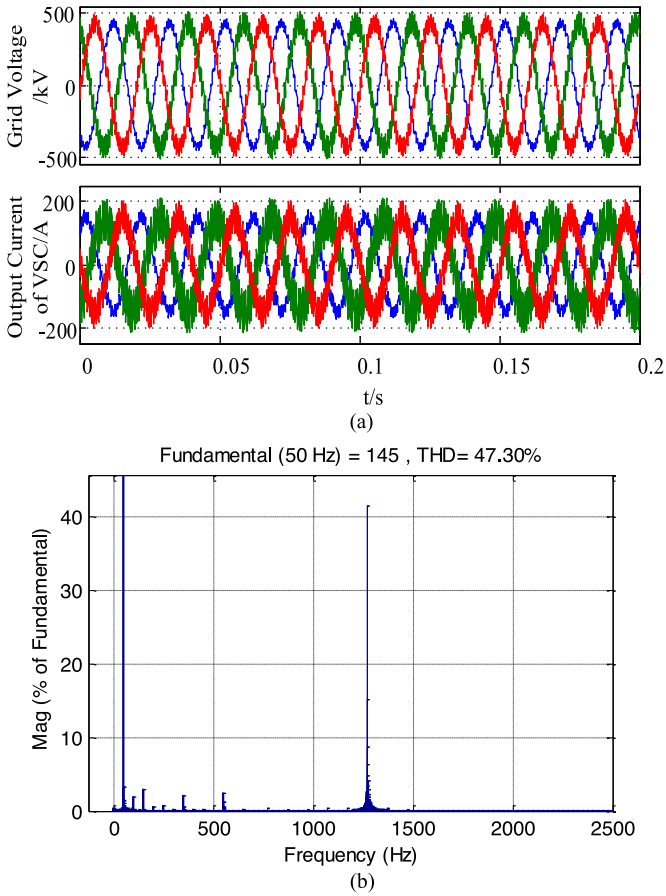

Fig. 15. 1270 Hz resonance occurred in Luxi back-to-back VSC-HVDC. (a) The grid voltage and the output current of the VSC. (b) The FFT analysis result of phase B current.

IV. Discussion of Solutions

High-frequency resonance could gradually grow into a severe stability problem for grid operation if neglected. An acceptable solution must be found, otherwise, further development and application of VSC-HVDC in a bulk power system will be limited. Although the high-frequency resonance may occur only under specific ac system conditions, a limiting ac system operation mode is generally not a good solution as that is against the goal of constructing HVDC by utilities.

A. Improving Control Strategy

The VSC-HVDC ac impedance is highly related to delay in feedforward control because feedforward reacts to high-frequency and can be adverse when the delay is great enough. A direct and simple idea is to filter high-frequency signals in the feedforward path. For example, inserting a 200-Hz low-pass filter in the feedforward control, as shown in Fig. 16.

The ac impedance of VSC-HVDC turns to be

$$Z_{\text{active}} = \frac{sL + G_{\text{PI}}G_{d1}}{1 - G_{d2}G_{\text{filter}}} \tag{17}$$

where G_{filter} is the low-pass filter inserted in the feedforward path.

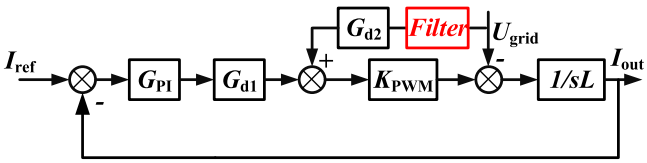

Fig. 16. Inserting an LP filter in the feedforward path to suppress the resonance.

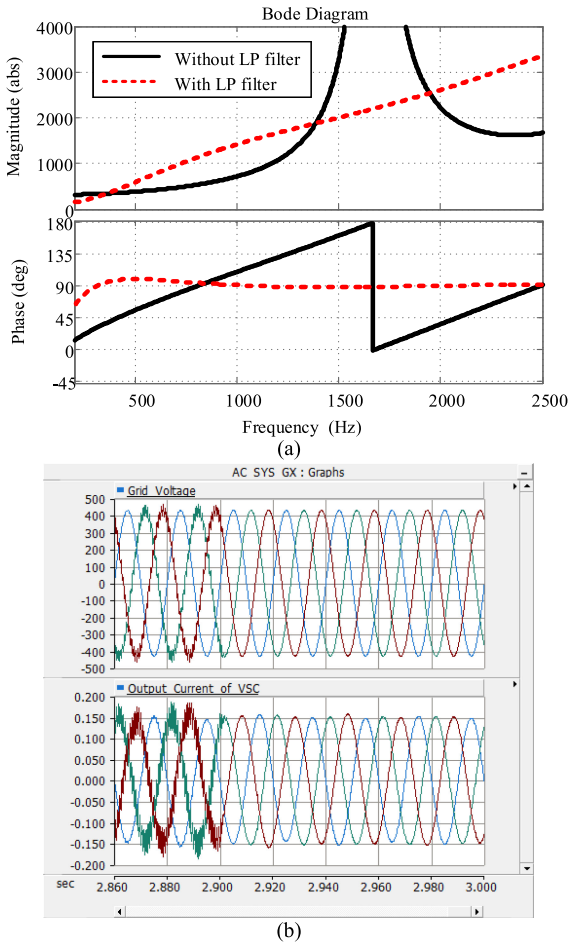

Fig. 17. Verification of the improving control strategy. (a) The Bode diagram of *Z*-active before and after a low-pass filter is inserted into the feedforward path. (b) Simulation result.

The Bode diagram of Z_{active} before and after the filter's insertion is shown in Fig. 17(a). The negative-real-part region has been greatly narrowed. According to the ac system impedance scan result, no high-frequency resonance should occur under all possible operation modes for Luxi project. The simulation results are shown in Fig. 17(b); the filter is inserted at 2.9 s and the resonance disappears immediately.

This method is applied in Luxi project, and numerous simulations have shown that resonance should not occur under all considered ac conditions and no resonance has occurred yet after adopting the new strategy. This can be an acceptable solution from project engineering perspective, but not an ideal solution as high-frequency resonance may still occur under some specific unpredicted ac system conditions as the negative-real-part region has not been eliminated.

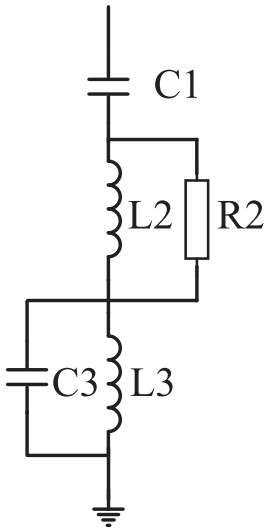

Fig. 18. A-type filter adopted in the Luxi station.

TABLE III
PARAMETERS AND VALUES OF THE A-TYPE FILTER

Parameters	Value
C_1/μF	1.3
L_2/mH	26.1
R_2/Ω	500.0
C_3/μF	2.4
L_3/mH	18.8

Similar solutions can be found, e.g., inserting notch filter in the feedforward path can help avoid resonance in a narrow frequency range, and therefore, a self-adapted notch filter may be a good choice. Such controller improving methods still need verification before applying in large-scale VSC-HVDC systems.

B. Connecting a Passive Impedance Adapter in Parallel

According to (13), the system stability changes when the passive element is connected in parallel, and stability criterion is as follows when one converter and one passive element are in service:

$$G_{\text{stability}} = \frac{Z_g}{Z_{\text{passive}}} + \frac{Z_g}{Z_{\text{active}}} = \frac{Z_g}{\frac{Z_{\text{passive}} Z_{\text{active}}}{Z_{\text{passive}} + Z_{\text{active}}}}. \quad (18)$$

To illustrate the influence of a passive impedance adapter, taking the A-type filter shown in Fig. 18, which is used in Luxi project as an example, the parameters of the filter are listed in Table III. The impedance of Z_{passive}, Z_{active}, and $Z_{\text{passive}}//Z_{\text{active}}$ are shown in Fig. 19. The negative-real-part region disappeared after applying an A-type filter, which guaranteed a good stability performance of the station. It should be noted that the outer control loops of VSC-HVDC are ignored, and the VSC-HVDC impedance in a low-frequency range may not be accurate.

For a VSC-HVDC station without a passive element, inserting a passive impedance adapter may be an option as the 525 kV

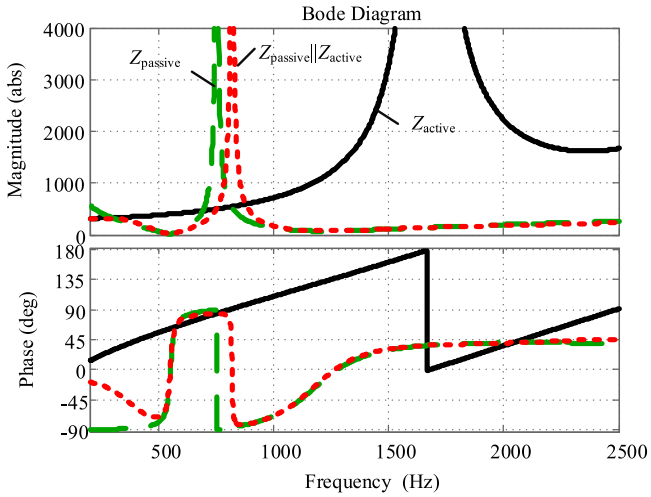

Fig. 19. Bode diagram of Z_{active}, $Z_{passive}$, and $Z_{active}//Z_{passive}$.

passive elements are technically and economically mature for applications. Unlike passive damping methods used in *LCL*-type filters, a well-designed passive impedance adapter causes little power loss.

C. Connecting a Small-Scale Converter in Parallel

For small-scale converters with a small control delay, its ac impedance can be controlled in a larger frequency range. Similar to connecting a passive impedance adapter, such method may be applicable. However, connecting a small-scale converter to the 525 kV grid may need a step-up transformer, which needs to be further studied.

D. System Stability When Lots of Equipment Are Considered

In the analysis mentioned above, only the VSC-HVDC and one adapter are considered. In reality, other equipment besides the concerned VSC-HVDC and the adapter may exist, e.g., more than one ac filter could be connected when LCC-HVDC is in service. Z_{eq} changes every time when any of the equipment is put into service or cut off. The number of equipment combinations can be enormous, thus making analysis quite time consuming and exhausting. To simplify the analysis, the equipment should be divided into several sectors.

In this paper, the whole system is divided into two parts: the grid (Z_g) and the equipment (Z_{eq}), as shown in Fig. 20. For the equipment, more than two elements are considered. Dividing the *n* equipment into *m* sectors, it can be proven that

$$iZ_A, Z_B \in (-90^\circ, +90^\circ) \Rightarrow Z_{AB} = \frac{Z_A Z_B}{Z_A + Z_B} \in (-90^\circ, +90^\circ). \quad (19)$$

Consequently, Z_{eq} has a positive-real-part if impedance of each sector has a positive-real-part. Thus, the state change of each sector whose impedance has a positive-real-part should not deteriorate system stability, and the problem is simplified. By doing so, there is no need to analyze all possible combinations of the equipment in service. Every time an active element is connected, the operator should check its impedance. During the check, inserting an adaptor or assigning an element to compose a subsector may be necessary. For the checked subsectors, there is no need to double check again.

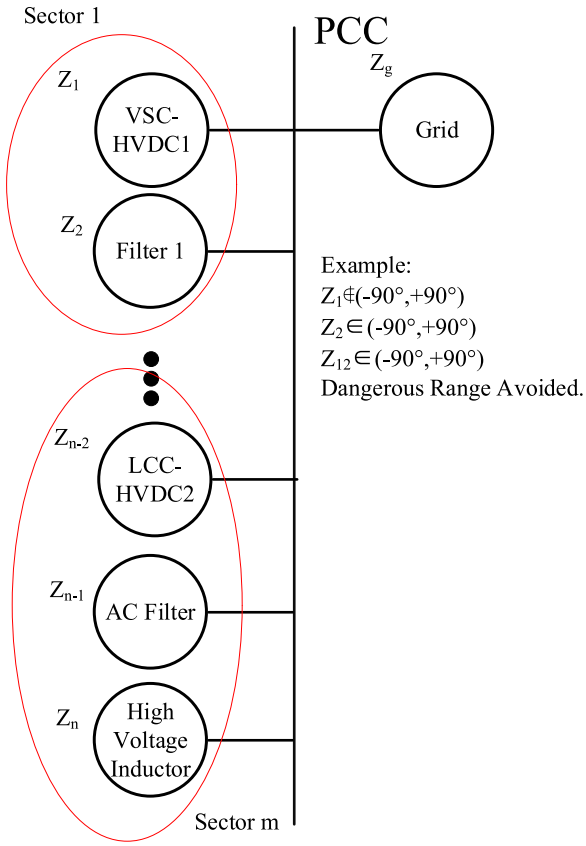

Fig. 20. System stability analysis model.

For each equipment containing a negative-real-part region, a new equipment or the existing equipment should be assigned to the sector to eliminate the negative-real-part region.

V. Conclusion

This paper discusses the resonance between a VSC-HVDC converter and the ac grid. The system stability analysis model considering different equipment is established and the system stability is judged by the ratio of the grid impedance to the equivalent impedance of all parallel-connected equipment. The 1270 Hz resonance case occurred in Luxi VSC-HVDC project is analyzed using the criterion and the phenomena are repeated in the simulation. The impedance of VSC-HVDC has a negative-real-part in a high-frequency range due to its instantaneous feed-forward and long control delay, and such characteristics result in a high-frequency resonance when several ac lines are cut off.

The negative-real-part region can be used to evaluate the risk of resonance. Improving control strategy, inserting passive impedance adapter, and inserting active impedance adapter may be applicable to narrow or eliminate the negative-real-part region. The design of high-voltage active impedance adapter and control strategy improving methods need further study.

For a complex system containing lots of equipment, by dividing them into several subsectors, system stability can be guaranteed by avoiding the negative-real-part region for each subsector. By doing so, there is no need to analyze all possible combinations of running equipment.

REFERENCES

[1] F. A. R. Jowder and B. T. Ooi, "VSC-HVDC station with SSSC characteristics," *IEEE Trans. Power Electron.*, vol. 19, no. 4, pp. 1053–1059, Jul. 2004.

[2] M. Amin, M. M. J. Lyu, and X. Cai, "Impact of power flow direction on the stability of VSC-HVDC seen from the impedance Nyquist plot," *IEEE Trans. Power Electron.*, vol. 32, no. 10, pp. 8204–8217, Oct. 2017.

[3] G. P. Adam, I. A. J. E. Fletcher, G. M. Burt, D. Holliday, and S. J. Finney, "New efficient submodule for a modular multilevel converter in multiterminal HVDC networks," *IEEE Trans. Power Electron.*, vol. 32, no. 6, pp. 4258–4278, Jun. 2017.

[4] P. M. Meshram and V. B. Borghate, "A simplified nearest level control (NLC) voltage balancing method for modular multilevel converter (MMC)," *IEEE Trans. Power Electron.*, vol. 30, no. 1, pp. 450–462, Jan. 2015.

[5] Q. Song, W. L. X. Li, H. Rao, S. Xu, and L. Li, "A steady-state analysis method for a modular multilevel converter," *IEEE Trans. Power Electron.*, vol. 28, no. 8, pp. 3702–3713, Aug. 2013.

[6] M. Liserre, F. Blaabjerg, and S. Hansen, "Design and control of an LCL-filter-based three-phase active rectifier," *IEEE Trans. Ind. Appl.*, vol. 41, no. 5, pp. 1281–1291, Sep./Oct. 2005.

[7] T. C. Y. Wang, Z. Ye, G. Sinha, and X. Yuan, "Output filter design for a grid-interconnected three-phase inverter," in *Proc. Power Electron. Spec. Conf.*, 2003, pp. 779–784.

[8] R. Pena-Alzola, M. Liserre, F. Blaabjerg, R. Sebastian, J. Dannehl, and F. W. Fuchs, "Analysis of the passive damping losses in LCL-filter-based grid converters," *IEEE Trans. Power Electron.*, vol. 28, no. 6, pp. 2642–2646, Jun. 2013.

[9] I. J. Gabe, V. F. Montagner, and H. Pinheiro, "Design and implementation to the grid through an LCL filter," *IEEE Trans. Power Electron.*, vol. 24, no. 6, pp. 1444–1452, Jun. 2009.

[10] R. Pena-Alzola, M. Liserre, F. Blaabjerg, R. Sebastian, J. Dannehl, and F. W. Fuchs, "Systematic design of the lead-lag network method for active damping in LCL-filter based three phase converters," *IEEE Trans. Ind. Informat.*, vol. 10, no. 1, pp. 43–52, Feb. 2014.

[11] J. Dannehl, M. Liserre, and F. W. Fuchs, "Filter-based active damping of voltage source converters with LCL filter," *IEEE Trans. Ind. Informat.*, vol. 58, no. 8, pp. 3623–3633, Aug. 2011.

[12] C. Zou, B. Liu, S. Duan, and R. Li, "Influence of delay on system stability and delay optimization of grid-connected inverters with LCL filter," *IEEE Trans. Ind. Informat.*, vol. 10, no. 3, pp. 1775–1784, Aug. 2014.

[13] D. Pan *et al.*, "Capacitor-current-feedback active damping with reduced computation delay for improving robustness of LCL-type grid-connected inverter," *IEEE Trans. Power Electron.*, vol. 29, no. 7, pp. 3414–3427, Jul. 2014.

[14] J. Sun, "Impedance-based stability criterion for grid-connected inverters," *IEEE Trans. Power Electron.*, vol. 26, no. 11, pp. 3075–3078, Nov. 2011.

[15] B. Wen, D. Boroyevich, R. Burgos, P. Mattavelli, and Z. Shen, "Inverse Nyquist stability criterion for grid-tied inverters," *IEEE Trans. Power Electron.*, vol. 32, no. 2, pp. 1548–1556, Feb. 2017.

[16] M. Cespedes and J. Sun, "Mitigation of inverter-grid harmonic resonance by narrow-band damping," *IEEE J. Emerging Select. Topics Power Electron.*, vol. 2, no. 4, pp. 1024–1031, Oct. 2014.

[17] L. Harnefors, M. Bongiorno, and S. Lundberg, "Input-admittance calculation and shaping for controlled voltage-source converters," *IEEE Trans. Ind. Electron.*, vol. 54, no. 6, pp. 3323–3334, Dec. 2007.

[18] L. Harnefors *et al.*, "Passivity-based stability assessment of grid-connected VSC: An overview," *IEEE J. Emerging Select. Topics Power Electron.*, vol. 4, no. 1, pp. 116–125, Mar. 2016.

[19] L. Harnefors *et al.*, "Passivity-based stabilization of resonant current controllers with consideration of time delay," *IEEE Trans. Power Electron.*, vol. 29, no. 12, pp. 6260–6263, Dec. 2014.

[20] L. Harnefors *et al.*, "Passivity-based controller design of grid-connected VSCs for prevention of electrical resonance instability," *IEEE Trans. Ind. Electron.*, vol. 62, no. 2, pp. 702–710, Feb. 2015.

[21] L. Harnefors, L. Zhang, and M. Bongiorno, "Frequency-domain passivity-based current controller design," *IET Power Electron.*, vol. 1, no. 4, pp. 455–465, 2008.

[22] L. Harnefors, R. Finger, X. Wang, H. Bai, and F. Blaabjerg, "VSC input-admittance modeling and analysis above the Nyquist frequency for passivity-based stability assessment," *IEEE Trans. Ind. Electron.*, vol. 64, no. 8, pp. 6362–6370, Aug. 2017.

[23] X. Wang, F. Blaabjerg, and P. C. Loh, "Passivity-based stability analysis and damping injection for multiparalleled VSCs with LCL filters," *IEEE Trans. Power Electron.*, vol. 32, no. 11, pp. 8922–8935, Nov. 2017.

[24] K. Sharifabadi *et al.*, *Design Control and Application of MMC for HVDC Transmission System*. Hoboken, NJ, USA: Wiley, Aug. 2016. [Online]. Available: http://www.wiley.com

[25] J. Sun and H. Liu, "Sequence impedance modeling of modular multilevel converters," *IEEE J. Emerging Select. Topics Power Electron.*, vol. 5, no. 4, pp. 1427–1443, Dec. 2017.

[26] B. Wen, D. Boroyevich, R. Burgos, P. Mattavelli, and Z. Shen, "Analysis of D-Q small-signal impedance of grid-tied inverters," *IEEE Trans. Power Electron.*, vol. 31, no. 1, pp. 675–687, Jan. 2016.

[27] M. Cespedes and J. Sun, "Impedance modeling and analysis of grid-connected voltage-source converters," *IEEE Trans. Power Electron.*, vol. 29, no. 3, pp. 1254–1261, Mar. 2014.

[28] C. Zou, B. Liu, S. Duan, and R. Li, "A feedforward scheme to improve system stability in grid-connected inverter with LCL filter," in *Proc. Energy Convers. Congr. Expo.*, 2013, pp. 4476–4480.

[29] Z. Yang *et al.*, "Study on harmonic impedance equivalents used for ac filter design of ±800 kV UHVDC transmission project from Xiangjiaba to Shanghai," *Power Syst. Technol.*, vol. 31, no. 18, pp. 1–4 + 14, 2007 (in Chinese).

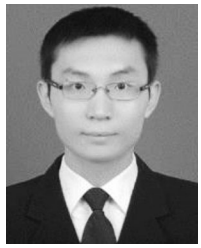

Changyue Zou (M'17) received the B.S. and Ph.D. degrees in electrical engineering from the Huazhong University of Science and Technology, Wuhan, China, in 2010 and 2015, respectively.

He is currently an Electrical Engineer with the Electric Power Research Institute, China Southern Power Grid Co., Ltd., Guangdong, China. His main research interests include control and design of voltage source converter-high-voltage dc.

Hong Rao (SM'12) received the B.S. degree in electrical engineering from the Huazhong University of Science and Technology, Wuhan, China, in 1983.

He is currently the Director with the Electric Power Research Institute, China Southern Power Grid Co., Ltd., Guangdong, China, and the Chief Specialist with China Southern Power Grid Co., Ltd. His main research interests include the design of advanced high-voltage dc based projects and operation of bulk ac/dc power system.

Mr. Rao is a Committee Member of ClGRE SC B4. He was the recipient of the first prize of the National Science and Technology Progress Award, the first prize of China Electric Power Science and Technology Progress Award, and the Outstanding Contribution to China Electric Power Science and Power Technology Award.

Shukai Xu (M'13) received the B.S. and Ph.D. degrees in electrical engineering from Tsinghua University, Beijing, China, in 2002 and 2007, respectively.

He is currently the Deputy Director with the HVDC and Power Electronics Department, Electric Power Research Institute, China Southern Power Grid Co., Ltd., Guangdong, China, and the Deputy Executive Director with the State Key Laboratory of HVDC. His main research interests include control and the design of voltage source converter-high-voltage dc and flexible ac transmission system.

Yan Li (M'12) received the B.S., M.S., and Ph.D. degrees in electrical engineering from the Huazhong University of Science and Technology, Wuhan, China, in 1996, 1999, and 2003, respectively.

He is currently the Director with the HVDC and Power Electronics Department of Electric Power Research Institute, China Southern Power Grid Co., Ltd., Guangdong, China, and the Deputy Executive Director with the State Key Laboratory of HVDC. His main research interests include control and design of line-commutated converter-voltage source converter and voltage source converter-high-voltage dc.

Weiwei Li (M'12) received the B.S. and Ph.D. degrees in electrical and electronic engineering from the Huazhong University of Science and Technology, Wuhan, China, in 2009 and 2014, respectively.

He is currently an Electrical Engineer with the Electric Power Research Institute, China Southern Power Grid Co., Ltd., Guangzhou, China. His research interests include digital control techniques and renewable-energy generation systems.

Jun Chen (M'17) received the B.S. and M.S. degrees in electrical engineering from the Huazhong University of Science and Technology, Wuhan, China, in 2009 and 2012, respectively.

He is currently an Engineer with the Electric Power Research Institute, China Southern Power Grid Co., Ltd., Guangzhou, China. His main research interests include voltage source converter-high-voltage dc and power electronic systems.

Xiaobin Zhao received the B.S. degree in electrical engineering from the Huazhong University of Science and Technology, Wuhan, China, in 2008.

He is currently an Engineer with the Electric Power Research Institute, China Southern Power Grid Co., Ltd., Guangdong, China. His main research interests include power system analysis, ac and dc filter design, overvoltage, and insulation coordination research of high-voltage dc.

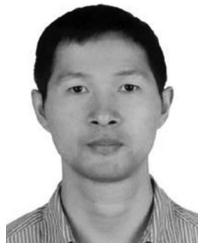

Yu Yang received the B.S. and Ph.D. degrees in electrical engineering from Shanghai Jiaotong University, Shanghai, China, in 1995 and 2000, respectively.

He is currently an Engineer with the Electric Power Research Institute, China Southern Power Grid Co., Ltd., Guangdong, China. His main research interests include power system analysis, and control and design of high-voltage dc.

Bo Lei received the B.S. and M.S. degrees in electrical engineering from Hunan University, Changsha, China, in 2011 and 2014, respectively.

He is currently an Engineer with the Electric Power Research Institute, China Southern Power Grid Co., Ltd., Guangdong, China. His main research interests include design of voltage source converter-high-voltage dc and application of battery energy storage system.